Food Research International 160 (2022) 111742

Contents lists available at ScienceDirect

Food Research International

journal homepage: www.elsevier.com/locate/foodres

# The anti-inflammatory effect of vasoactive peptides from soybean protein hydrolysates by mediating serum extracellular vesicles-derived miRNA-19b/CYLD/TRAF6 axis in the vascular microenvironment of SHRs

Tianyuan Song [a], Minzhi Zhou [a], Wen Li [a], Miao Lv [a], Lin Zheng [a,b,*], Mouming Zhao [a,b,*]

[a] School of Food Science and Engineering, South China University of Technology, Guangzhou 510640, PR China
[b] Chaozhou Branch of Chemistry and Chemical Engineering Guangdong Laboratory, Chaozhou 521000, PR China

ARTICLE INFO

*Keywords:*
Hypertension
Anti-inflammatory
Soybean peptides
Extracellular vesicles
Spontaneously hypertensive rat

ABSTRACT

The excessive accumulation of angiotensin II (Ang II) in the vascular microenvironment promotes vascular dysfunction including vascular endothelial inflammation and remodeling. In the present study, a soybean protein hydrolysate enriching with vasoactive peptides was prepared and explored the anti-inflammatory effects on the aorta of spontaneous hypertensive rats (SHRs). The soybean-derived vasoactive peptide (SVP) significantly reduced the blood pressure and attenuated inflammation of the aorta in SHRs. Pathologically, the SVP improved the wall thickening and inflammatory cell infiltration of the aorta. Mechanistically, the SVP not only reduced the expression of miRNA-19b in the aorta but down-regulated the packaging of miRNA-19b in serum EVs. The miRNA-19b targeted the deubiquitinating enzyme cylindromatosis (CYLD) in the aorta and broke the ubiquitination balance of CYLD-TRAF6. These results caused a disorder of the TRAF6-mediated signaling pathway in the aorta, which resulted in upregulation of the expression of IL-6 and TNF-α in the aorta. This pathological process in SHRs was improved by the SVP hydrolysate gavage administration. These results reported a novel anti-inflammatory mechanism of SVP through the serum EVs mediating the miR-19b/CYLD/TRAF6 axis.

## 1. Introduction

As the most common cardiovascular disease (CVD), hypertension has become a major risk factor for death worldwide. Studies have shown that vascular dysfunction is directly related to the occurrence and development of hypertension (García-Tejedor et al., 2017; Virdis, Dell'Agnello, & Taddei, 2014; Virdis & Schiffrin, 2003). Angiotensin II (Ang II), a vasoconstrictor from the hyperactive renin-angiotensin-aldosterone system (RAAS), is reported to promote vascular remodeling and endothelial dysfunction in hypertension (Utsunomiya et al., 2011). A series of studies demonstrated that the Ang II-induced vascular inflammation would exacerbate vascular dysfunction, but the potential molecular mechanism is still not clear (Virdis et al., 2014; C. Yang et al., 2020). Both vascular endothelial cells (VECs) and vascular smooth muscle cells (VSMCs), as the main components of the vascular wall, have an important impact on the function of blood vessels (Hu et al., 2021). Recent research demonstrated that the Ang II-mediated vascular dysfunction in the vascular microenvironment would be directly related to intercellular communication between VECs and VSMCs (La Salvia, Gunasekaran, Byrd, & Erdbrügger, 2020).

The extracellular vesicles (EVs) are membranous subcellular particles, and the diameter of EVs in general is ~30 to ~200 nm. They have been defined as a novel messenger for cell-to-cell or organ-to-organ communication (Reiner & Somoza, 2019). A series of bioactive molecules including proteins, nucleic acids, and lipids were loaded in EVs, which are potential indicators of the dysfunction of donor cells (Paolicelli, Bergamini, & Rajendran, 2019). Numerous researches published that EVs participated in vascular homeostasis by regulating vascular inflammation and oxidative stress (Bodega, Carracedo, & Ramírez, 2019; La Salvia et al., 2020). The microRNA molecular (miRNA), a small and specific non-coding RNA, was found to be abundantly enriched in EVs and exert its biological function by suppressing gene expression in recipient cells (Fang et al., 2018). Based on this mechanism, some miRNAs were certified to play an important role in vascular disease. The miRNA-223-3p was reported to inhibit vascular calcification and the osteogenic switch of VSMCs (Han et al., 2021). The miR-143/145 were overexpressed in the EVs secreted by KLF2-transduced or shear-stress-induced human umbilical vein endothelial cells (HUVECs) and

* Corresponding authors.
*E-mail addresses:* linzheng18@163.com (L. Zheng), femmzhao@scut.edu.cn (M. Zhao).

https://doi.org/10.1016/j.foodres.2022.111742
Received 12 February 2022; Received in revised form 21 July 2022; Accepted 24 July 2022
Available online 28 July 2022

targeted some gene expression of VSMCs, which were regarded as promising evidence of atherosclerosis (Hergenreider et al., 2012). A recent study indicated that the miR-146a was an NF-κB-dependent gene and regulated the inflammation-related Toll-like receptors (Taganov, Boldin, Chang, & Baltimore, 2006).

Some studies demonstrated that the natural bioactive products could affect the biological functions of EVs by altering the EVs-loading miRNAs. The *Dendrobium officinale* polysaccharide (DOP) was reported to improve intestinal inflammation by regulating the miR-433-3p packaging in intestinal cells-derived EVs (H. Liu et al., 2021). Paeonol isolated from *Cortex Moutan* radix showed an ameliorating effect on the inflammatory response of HUVECs by mediating miR-223 in monocytes-derived EVs (Y. Liu et al., 2018). Our previous studies first reported that casein-derived antihypertensive peptides Val-Pro-Pro and Ile-Pro-Pro could regulate the biological function of small EVs from Ang II-induced VSMCs or HUVECs (Song, Lv, Sun, Zheng, & Zhao, 2020; Song, Lv, Zhang, et al., 2020). Moreover, we also found that soybean protein-derived antihypertensive tripeptide Leu-Ser-Trp attenuated Ang II-induced endothelial dysfunction by altering miRNAs packaging in the VSMCs-derived EVs (Song et al., 2021). However, the *in vivo* mechanisms of these peptides are still unclear.

Soybean protein has been treated as an excellent natural library of biopeptide. The soybean protein-derived peptides were reported to be nutritional supplementation and improve certain chronic diseases such as hypertension, hyperlipidemia, and diabetes (I. S. Kim, Yang, & Kim, 2021). In *vitro* fermentation, enzymatic hydrolysis, and food processing are the main methods of preparation of peptides (Barati et al., 2020; Chatterjee, Gleddie, & Xiao, 2018; Tu et al., 2014). Numerous researchers reported some beneficial effects of soybean-derived biopeptides on the cardiovascular system through various mechanisms (Gu & Wu, 2013). The tripeptide Leu-Ser-Trp was first found to improve the Ang II-induced VSMCs inflammation through mediating AT1R (angiotensin type I receptor) expression and ERK1/2 (extracellular signal-regulated kinases 1 and 2) phosphorylation (Lin, Liao, Bai, Wu, & Wu, 2017). Recently, our lab has identified some novel ACE-inhibitory peptides from soybean protein hydrolysate and verified the binding model by *in silico* molecular docking (Xu et al., 2021). However, the knowledge about *in vivo* activity of soybean protein-derived hydrolysate is still lacking. Therefore, this study primarily explored a novel EVs-mediated improvement of soybean protein-derived hydrolysate on vascular inflammation of spontaneously hypertensive rats (SHRs).

## 2. Materials and methods

### 2.1. Chemicals

Cell medium DMEM, phosphate-buffered saline (PBS, basic 1 ×, pH 7.4), and fetal bovine serum (FBS, #10099141C) were obtained from Gibco™ (Carlsbad, CA, USA). Trypsin and antibiotics (penicillin/streptomycin) solution were purchased from Sigma-Aldrich (St. Louis, MO). Serum-free media (for exosome culture) was obtained from Umibio (Shanghai, China) Co. Ltd. The cell lines HUVECs (CRL-1999) were obtained from ATCC (Manassas, VA, USA). Endothelial cell-specific medium (ECM) and endothelial cell growth supplement (ECGS) were purchased from ScienCell (San Diego, CA). Protex was obtained from Novozyme Biotechnology Co. Ltd (Beijing, China). Ang II was purchased from Solarbio (Beijing, China). DAPI solution was purchased from the Beyotime Institute of Biotechnology (Shanghai, China). Phalloidin green fluorescent and PKH26 red fluorescent were purchased from Sigma Aldrich (St Louis, MO, USA). The ELISA kits for rats TNF- α and IL-6 were purchased from Solarbio Life Science Company (Beijing Solarbio Science & Technology Co., Ltd.). The BCA protein assay kit was purchased from Thermo Fisher Scientific Pierce™. Antibodies against Tsg 101 (ab125011), Calnexin (ab22595), CYLD (ab137524), TRAF6 (ab40675), IκB-alpha (ab32518) were purchased from Abcam (Cambridge, UK). Antibodies against CD9 (Cat No. 20597), CD81(Cat No. 66866-1-Ig), GAPDH (Cat No. 10494-1-AP), p65 (Cat No. 10745-1-AP) were purchased from Proteintech (Chicago, IL, USA).

### 2.2. Ethics statement

All the animal experiments in this study conformed to the relevant provisions of the Animal Nursing and Use Committee (Approval ID: SYXK(Yue) 2021-0726). All efforts were made to reduce animal pain as much as possible.

### 2.3. Preparation of SVP

The soybean protein-derived vasoactive peptide (SVP) was prepared as described previously with some modifications (Xu et al., 2021). Briefly, soybean protein isolate (SPI) was equably suspended in distilled water and then the mixture was hydrolyzed by alcalase and flavourzyme (final concentration: 1%, w/w) at pH 7.5 for 8 h, respectively. Subsequently, the enzymic reaction was terminated by heating the samples in boiling water for 15 min. The hydrolysis was cooled in an ice bath and centrifuged at 9000*g* for 20 min using a centrifuge. The supernatants were achieved and spray-dried to obtain SVP, and the SVP powder was stored at −20 °C.

### 2.4. Animals and experimental protocol

The vasoactive effect of SVP was assessed using SHR and WKY model. Twenty-four pathogen-free male SHRs (10-week-old) and six pathogen-free male WKYs (10-week-old) were purchased from Vital River Experimental Animal Technical Co. Ltd. (Beijing China). Both SHRs and WKYs were housed under a 12 h light–dark cycle at 24 °C, and they were allowed access to food and tap water *ad libitum*. Then, the rats were randomly divided into 5 groups (n = 6 each): MD group, SHRs with no special feeding treatment; BC group, WKYs with no special feeding treatment; CP group, SHRs were orally gavaged with captopril at 20 mg/kg·BW each day; SVPL group, SHRs have orally gavaged with 100 mg/kg·BW SVP hydrolysate each day; and SVPH group, SHRs were orally gavaged with 500 mg/kg·BW SVP hydrolysate each day. The gavage dose refers to the human equivalent dosage based on body surface, and the conversion factor between adults (~70 kg·BW) and rats (~250 g·BW) was used in experiment (Nair & Jacob, 2016). The blood pressure was measured by a tail-cuff system (BP 2000, Visitech Systems, USA) as previously described (Pan et al., 2018). The BP measurements were performed during the daytime (12:00p.m. to 6:00p.m.) after the previous 3 days of training. Blood pressure was measured every two days; at least 15 effective values were recorded at each point.

Simultaneously, additional WKYs were randomly divided into 3 groups (n = 6) to test the effects of SVP hydrolysate on BP of normotensive WKYs: $BC_{WKY}$ group, WKYs with no special feeding treatment; $CP_{WKY}$ group, orally gavaged with at 20 mg/kg·BW captopril each day; $SVP_{WKY}$ group, orally gavaged with 500 mg/kg·BW SVP hydrolysate each day. The same method is used to monitor the BP of WKYs. On the last day of the experimental period, three groups WKYs were infused subcutaneously with Ang II (200 ng/kg/min) via tail vein, and the blood pressure change was monitored within 24 h.

All measurements were performed by the same person in the same environment at the same time of day to reduce measurement error. After 4 weeks, rats were fasted overnight and intraperitoneally injected with chloral hydrate solution (15 %) in a ratio of 4 mL/kg body weight for anesthesia. The aorta was then immediately excised and fixed in 10 % formaldehyde overnight, embedded in paraffin, and stored at −80 °C until analysis of the expression of protein by western blot. Blood samples were collected from the abdominal vein (portal) immediately in tubes, and serum was separated from the blood by centrifugation at 1000*g* for 15 min and then stored at −20 °C for further assays. The experimental kits were used to determine the content of TNF-α and IL-6 in serum.

### 2.5. Echocardiography

Rats were fixed at a platform and anesthetized by inhaling isoflurane (5% for induction and 2–2.5 % for maintenance). After the reflex of the hind limbs disappears, the supine position is fixed on the 37 °C constant temperature physiological information monitoring table, the limbs are fixed on the metal detector after applying a small amount of coupling, and the transthoracic ultrasound detection is carried out after hair removal on the left chest. A Vevo 2100 high-resolution small animal ultrasound imaging system (Vevo®2100; Vivo SONIC, Toronto, ON, Canada) was employed for imaging. The device uses a broadband linear array probe (MS-400) with a frequency of 30 MHz. The probe is placed on the left chest of the rat, rotated 30–45° towards the right shoulder of the rat, B-Mode can see the left ventricular long-axis section; the probe is rotated clockwise 90° to show the left ventricular short axial section, the M-Mode ultrasound is applied to the largest section of the papillary muscle to record the left ventricular movement, record the heart rate (HR), measure the thickness of the anterior wall of the left ventricle during the diastolic phase (LVAWd), and the thickness of the posterior wall of the left ventricle during the diastolic period (LVPWd), Left ventricular end-diastolic inner diameter (LVEDd) and left ventricular end-systolic diameter (LVESd); each rat was measured 3 times, taking the average of 3 cardiac cycles. After the completion of the experiment, the data analysis was performed, and the left ventricular ejection fraction (EF) of the heart was calculated according to the results of the ultra-long axis section, and the shortening rate (FS) of the left ventricle of the heart calculated according to the results of the ultra-long axis tangent. All results were monitored by echocardiography.

### 2.6. Histological analysis

The thoracic aortas of rats were dissected and performed pathological analysis. The fixed aortas were sliced into 5 mm cross-sections and stained with hematoxylin-eosin (H&E) or Sirius red as previously described (Pan et al., 2018). All images were recorded using the Eclipse Ci-L microscope (Nikon, Tokyo, Japan), and were analyzed using Image-Pro Plus 6.0 software (Media Cybernetics, Rockville, MD, USA).

### 2.7. EVs isolation and characterization analysis

The small EVs were isolated from the serum of MD, BC, CP, and SVPH groups using a multi-step ultracentrifuge method described by M. Osada-Oka et al with a slight modification (Osada-Oka et al., 2017). The serum sample was centrifuged at 2000*g* for 30 min at 4 °C to remove cellular debris, and the supernatant was continued centrifuged at 10000*g* for 30 min at 4 °C. The supernatant was filtered through a 0.22 μm membrane and ultracentrifuged at 100000*g* for 1 h at 4 °C. The EVs at the bottom of the tube were washed in PBS at the same centrifugation, and then they were resuspended in 1 × PBS. The protein content was quantified through a BCA protein assay kit. The transmission electron microscope was used to observe the morphology of the EVs sample treated with paraformaldehyde and deposited on Formvar-carbon-coated EM grids. The analysis of EVs size was processed using a Nano-Sight NS3000 instrument as previously described (Andaluz Aguilar, Iliuk, Chen, & Tao, 2019). Three classical transmembrane proteins (CD9, CD81, and Tsg101) were detected as the biomarker of EVs by the western blotting.

### 2.8. In vivo transplantation of EVs

To explore the *in vivo* function of EVs, we performed a tail vein injection of EVs sample into SHRs or WKYs, as in previous studies (H. Liu et al., 2021; Zhu et al., 2018). 15-week-old male SHR (n = 24) and WKY (n = 24) were purchased from Vital River Experimental Animal Technical Co. Ltd. The SHRs were randomly divided into four groups with EVs injection (20 μg protein in 100 μL PBS per rat): SHR + MDev, SHR + BCev, SHR + CPev, and SHR + SVPev. The WKYs performed the same operation. Rats are immediately monitored for BP changes within 4 h after EVs injection.

### 2.9. Quantitative RT-PCR and western blot analysis

Total RNA samples from tissue or EVs were obtained using the Invitrogen TRIzol reagent (Invitrogen, Thermo Fisher Scientific) according to the manufacturer's instructions. The RNA samples were recovered in DEPC solution and stored at −80 °C. The overall quality of RNA samples was estimated from OD260/OD280 ratio with a Nanodrop 2000 (Thermo Scientific, USA). Next, RNA (2 μg) were reverse transcribed by the synthesis of cDNA was performed using a Transcriptor First-Strand cDNA Synthesis System (Applied Biosystems, Branchburg, NJ). The primer sequences used for the real-time PCR analysis were as follows: miRNA-19b forward: 5′- GTCGTATCCAGTGCAGGGTCC-GAGGTATTCGCACTGGATACGAC-3′; miRNA-143 forward: 5′-CGCGTGAGATGAAGCACTG-3′; miRNA-145 forward: 5′- ACGGTC-CAGTTTTCCCAGGAATCCCT-3′; miRNA-155 forward: 5′-CAACG-GAAUCCCAAAAGCAGCUG-3′; U6 forward: 5′-CTCGCTTCGGC AGCACA-3′. For miRNA detection, a universal reverse primer from Invitrogen was used. RT-qPCR reactions were performed in a final system of 35 μL containing 2 μL of specific cDNAs. PCR amplification was carried out on a C1000 Touch Fast Real-Time PCR system (Bio-Rad) with the primers purchased from Guangzhou RiboBio Company. The fold change in the miRNA levels of each gene was calculated using the $2^{-\Delta\Delta Ct}$ method, with the housekeeping genes U6 as an internal control.

The protein expression was detected by western blot. Protein samples were prepared with radioimmunoprecipitation assay (RIPA) lysis buffer following standard protocols. The BCA protein assay kit was used to quantitate the lysis samples. The nucleoprotein was isolated with the Nucleoprotein Extraction Kit (#C500009, Sangon Biotech Co., Shanghai, China). Total proteins samples (40 μg protein/lane) were loaded onto sodium dodecyl sulfate–polyacrylamide gel electrophoresis (SDS-PAGE) gels, separated electrophoretically, and transferred to PVDF membranes. After blocking with 5 % dried skim milk for 2 h at room temperature, the membranes were incubated overnight at 4 °C with primary antibodies. The immunoreactive protein bands were visualized by ECL detection solution. The results were recorded by photographing with an Azure C300 Imaging System.

### 2.10. Cell culture and co-culture of EVs with HUVECs

The HUVECs were cultured in DMEM with 10 % FBS containing 100 U/mL penicillin and 100 g/mL streptomycin. Cells were grown to 70–80 % confluence and then treated with different sample incubations. Cells between passages 3 and 10 were used in this study.

### 2.11. EVs labeling and uptake

To further affirm whether serum EVs samples were taken up by HUVECs, the EVs labeling with PKH26 (a red fluorescent cell linker dye) was performed following the manufacturer's procedures. Briefly, the EVs (50 μg·protein) were resuspended in 500 μL of PBS with 100 μM PKH26 dye at 37 °C for 30 min. The HUVECs were seeded in a 6 well plate at a density of $1 \times 10^5$ cells/well, and incubated with the PKH26-labeled EVs at 37 °C for 6 h. Then, the HUVECs were washed with PBS and fixed with 4% paraformaldehyde for 15 min at room temperature. The HUVECs were permeabilized with 0.1% Triton X-100 for 15 min, and then DAPI was used to stain the cell nucleus (blue), and the phalloidin was used to mark the cytoskeleton. The signals were analyzed with a fluorescence microscope.

### 2.12. Knockdown of the deubiquitinating enzyme CYLD with siRNA

To silence the CYLD gene in HUVEC cells, the specific mixture of

three preselected siRNA duplexes to target different sequences of the human CYLD gene was utilized according to the manufacturer's instructions (Gao et al., 2010). The siRNA was mixed with Opti-MEM (Invitrogen, Carlsbad, CA) and Lipofectamine 3000 (ThermoFisher Scientific, USA) to form the transfection complex, before adding to the culture medium. Nonsilencing siRNA (SI03650325, Qiagen) with the same concentration was used as a negative control. The HUVECs were seeded in six-well plates at $1 \times 10^5$ cells/well, either CYLD siRNA or negative control siRNA (2 μmol/L) was added to the cells. The efficiency of gene silencing was determined by western blot 24 h after the treatments. CYLD and control small interfering RNAs (siRNAs) were synthesized by RiboBio (Guangzhou, China) and transfected into cells with the Lipofectamine 3000 reagent (Invitrogen).

### 2.13. Statistical analysis

Statistical analyses were performed for all results by the SPSS21.0 software package. All results data were presented as the mean ± SD unless otherwise specified. Differences between means were evaluated by one-way analysis of variance (ANOVA) for multiple comparison tests. $P < 0.05$ was defined as statistically significant.

## 3. Results

### 3.1. The SVP regulates the blood pressure of SHRs

The SHRs were administered SVP or captopril for 4 weeks by gavage to assess the effects of SVP on the blood pressure of SHRs, and the normotensive WKYs were selected as the control group. The variations in the BP of SHRs are displayed in Fig. 1, during the oral administration process, there was little change in SBP of WKY rats. The SBP of SHRs decreased slightly in the first week, but SBP of SHRs decreased significantly after 7 days, especially in the groups with captopril and SVP. After administration for 4 weeks, the maximal decrease in SBP was observed in the high-dose SVP group (SVPH), which declined by 72.47 mmHg compared to the initial value. Meanwhile, the captopril group (CP) and SVP low-dose group (SVPL) maintained a significant downward trend compared to the model group (MD). The body weight of rats slowly raised, and there was no significant difference in each group at the end of the experiment (Fig. 1 C). To examine the effect of SVP gavage on blood pressure in normotensive WKYs, the WKYs were assigned to three groups. Fig. 1 D and E showed changes in the SBP and DBP after oral SVP or captopril administration. The SVP had no significant effect on the BP of WKYs, and the BP of the $CP_{WKY}$ group showed a slight rise without a statistically significant (Fig. 1 D and E). After oral administration for 4 weeks, the Ang II injection could raise the SBP of the $CP_{WKY}$ and $SVP_{WKY}$

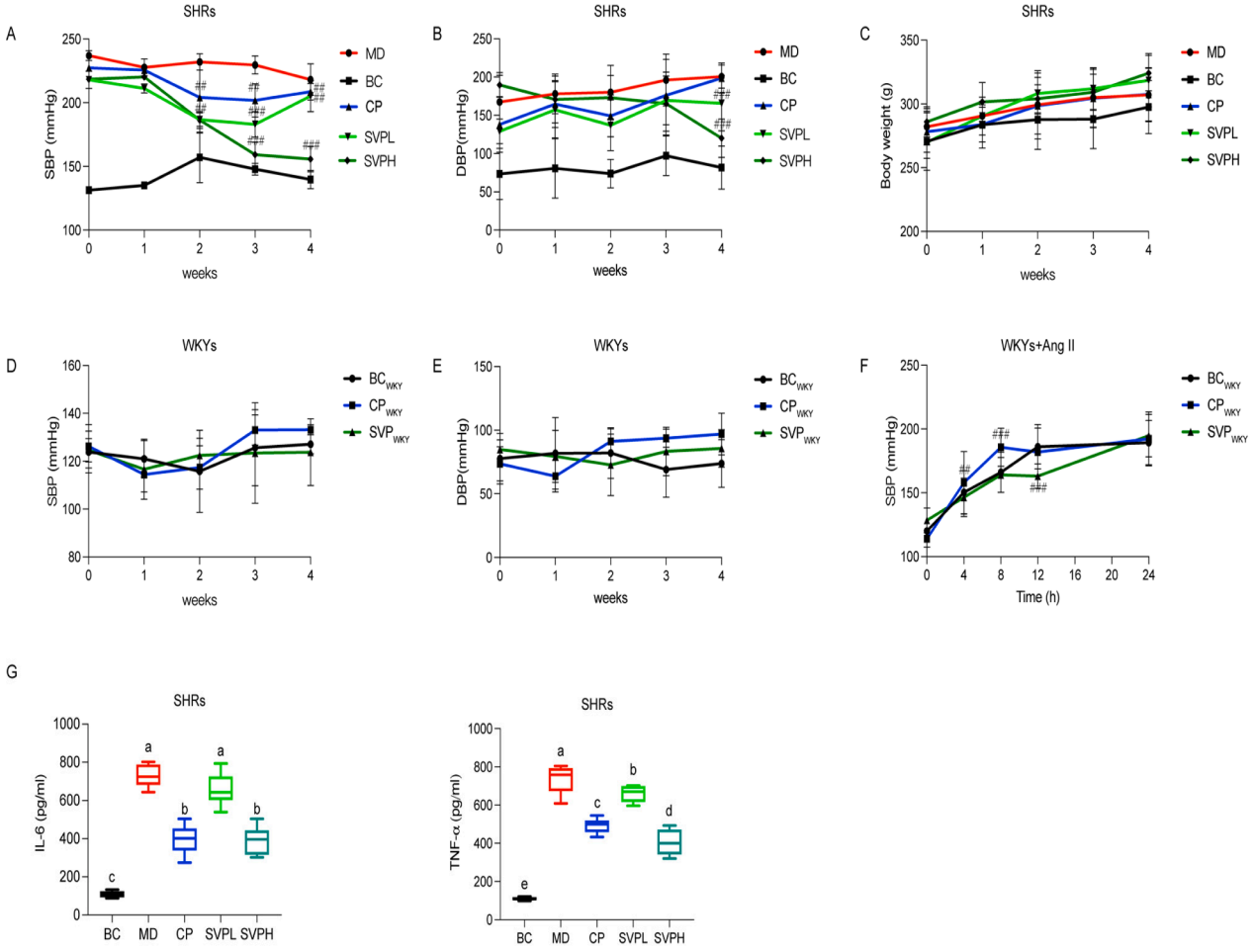


**Fig. 1. The soybean-derived vasoactive peptides reduce blood pressure and serum inflammatory cytokines of SHRs.** The systolic blood pressure (A), diastolic blood pressure (B), and body weight (C) in the spontaneously hypertensive rats (SHRs) treated with SVP or captopril. The systolic blood pressure (D) and diastolic blood pressure (E) in the normotensive WKYs rats treated with SVP or captopril. The Ang II increased systolic blood pressure (F) of SHRs with SVP or captopril pretreatment. The serum inflammatory cytokines IL-6 and TNF-α of SHRs treated with SVP or captopril. Values are expressed as mean ± SD (n = 6). ##P < 0.05 and ###P < 0.01 were labeled as WKYs *vs* SHRs; Graph bars with different letters on top represent statistically significant results (P < 0.05) based on ANOVA analysis, whereas bars labeled with the same letter correspond to results that show no statistically significant differences.

groups within 24 h. But the SBP augment the level of the $SVP_{WKY}$ group was lower than other groups within 12 h. This result showed that long-term oral administration of SVP would resist Ang II-induced BP rise. The results of the ELISA assay suggested that captopril and SVP could reduce the IL-6 and TNF- α cytokine of SHRs (Fig. 1 G). As shown in Fig. 2, echocardiography showed no significant difference in cardiac function and heart rate in different treatment groups (Fig. 2 A and B). But the Sirius red stain revealed that the heart of SHRs appeared to degenerate and infiltrate with the inflammatory cells, and the damage could be improved by SVP gavage (Fig. 2 A). These results indicated that SVP reduced the BP and inflammation of SHRs.

### 3.2. The histological and inflammatory analysis of aorta in SHRs

To investigate the effect of SVP in hypertensive vasculopathy, the vascular wall thickness and collagen fibrosis ratios were evaluated in thoracic aortas of SHRs and WKYs. The results of H&E staining showed that the aorta thickness of CP, SVPL, and SVPH groups was less than MD group after gavage administration for 4 weeks (Fig. 2 D). The wall thickness of the thoracic aorta in the SVPH group showed the most significant reduction (Fig. 2 E). The results of Sirius red staining demonstrated that compared with the BC group, the radio of fibrosis area in the MD group was significantly increased (Fig. 2 D). In addition, the collagen volume fraction of each group was calculated by Image J software (Fig. 2 C). The collagen deposition in the MD group was significantly higher than that of the BC group. Hence, these results illustrated that SVP and captopril significantly improved the aortic wall thickening and collagen deposition of SHRs, and the improvement effect of SVP gradually increases with the increase of concentration.

Since the previous experiment showed exacerbated inflammation in

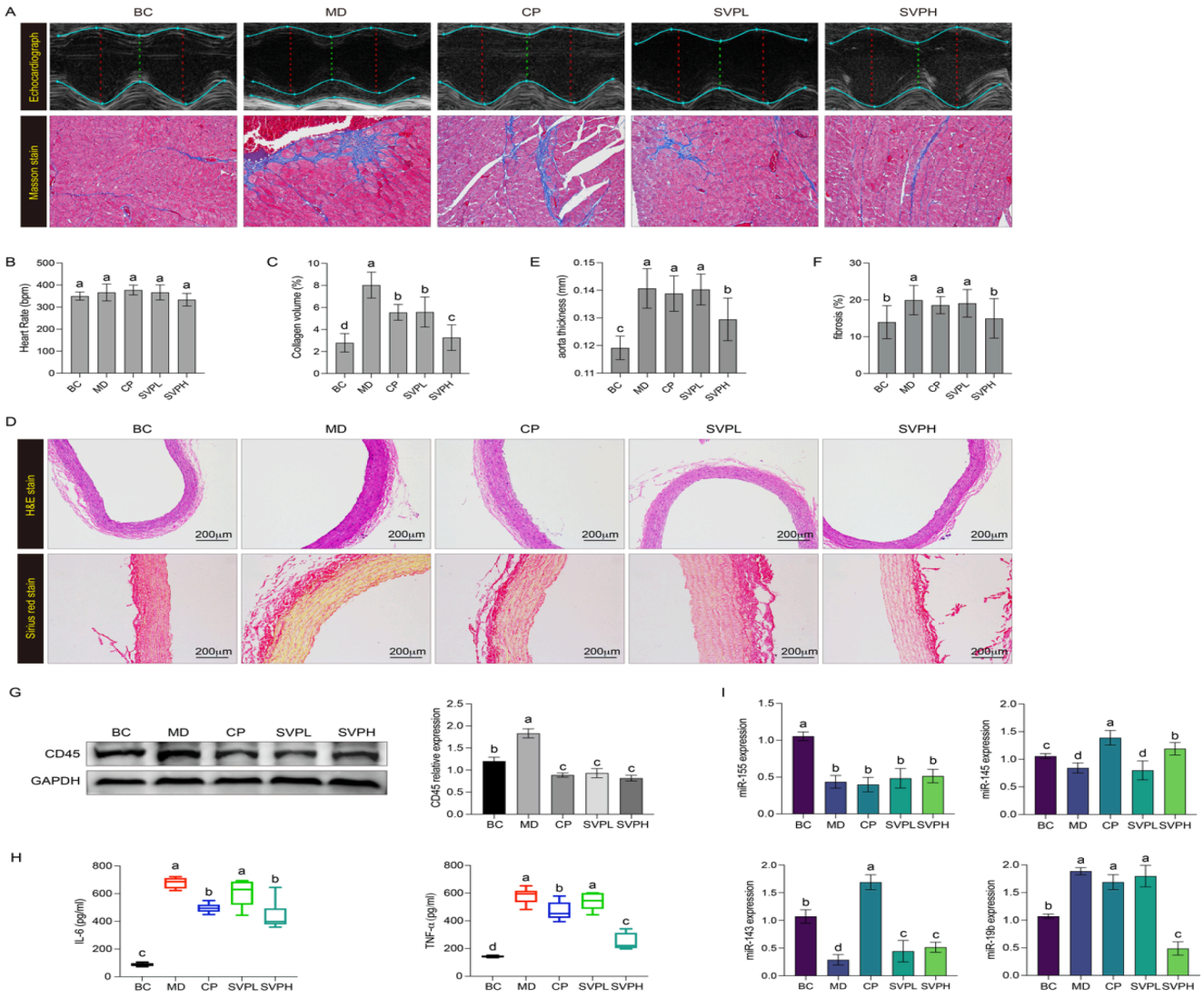


**Fig. 2. The soybean-derived vasoactive peptides regulated the vascular remodeling, inflammation, and miRNA expression of the aorta in SHRs.** (A) Representative echocardiograms measurement and Sirius red stain of heart in SHRs and WKYs with or without SVP treatment (n = 6). The images were visualized with optical microscopy at 400 × magnification. (B) Heart rate measurement of SHRs and WKYs (n = 6). (C) The percentage of heart collagen volume was analyzed by Image J software. (D) The H&E stain and Sirius red stain of the aorta in rats were imaged with optical microscopy at 100 × and 200 × magnification, respectively. (E) The aorta thickness was analyzed by Image J software. Measured in millimeters as the standard unit, the thickness of 5 aorta (mm) in each slice was measured separately and the average was calculated. (F) The aorta fibrosis percentage (%) was analyzed by Image J software. Percentage of the area of collagen fibers (%) was defined as pixel area of collagen fibers/tissue pixel area × 100. (G) The expression of CD45 in aorta of SHRs were detected by western blot. (H) The inflammatory cytokines IL-6 and TNF-α of the aorta were detected by ELISA. (I) The expression of miRNA-155, miRNA-145, miRNA-143, and miRNA-19b in the aorta of rats were tested by qRT-PCR. Values are expressed as mean ± SD (n = 6). Graph bars with different letters on top represent statistically significant results ($P < 0.05$) based on ANOVA analysis, whereas bars labeled with the same letter correspond to results that show no statistically significant differences. (For interpretation of the references to colour in this figure legend, the reader is referred to the web version of this article.)

SHRs, a reasonable view focused on the content of inflammatory factors in the aorta. The CD45, a biomarker of inflammatory cell infiltration, was over-expressed in the MD group. The captopril and SVP significantly reduced the expression of CD45 in aorta of SHRs (Fig. 2 G). ELISA assay revealed that both IL-6 and TNF- α were remarkably up-regulated in the MD group, and the captopril and high concentration SVP show similar ability to reduce levels of inflammatory factors (Fig. 2 H). Consistent with blood test results, SVP displayed a strong anti-inflammatory activity in the vascular microenvironment.

### 3.3. The SVP regulated differential miRNAs expression in the aorta

Vascular inflammation was confirmed to be directly related to endothelial dysfunction, and the miRNAs were regarded as a pivotal media for the endothelial function (Sun, Belkin, & Feinberg, 2013). The expression of four miRNAs, which have been verified to be associated with cardiovascular disease, was retested in these experiments (Fig. 2 I). The miR-155 is associated with VSMCs proliferation and vascular remodeling, and it was significantly downregulated in the aorta of SHRs, and either CP or SVP showed an aborted improvement. The miR-145, which is responsible for VSMCs phenotypes, was significantly downregulated in the MD group. The captopril exhibited better reversion to miR-145 expression than that of SVP. The miR-143 responded with Krüppel-like factor 2 (KLF2) mediating endothelial function, and it was reduced in the MD group. Interestingly, the miR-143 expression was increased by captopril but not SVP gavage administration. The SVP showed significant improvement in the overexpression of miR-19b in the aorta. However, captopril did not exert a similar effect on the overexpression of miR-19b. This result suggested that the SVP and CP have a similar ability to resist the expression of inflammatory factors (Fig. 2 G), but the mechanisms for regulating miRNAs in the aorta were different. Since miR-19b is the main regulator of SVP, the exploration of the molecular function of miR-19b may facilitate the elucidation of the anti-inflammatory mechanism of SVP *in vivo*.

### 3.4. Characterization of serum EVs

Serum EVs (SEVs) from SHRs and WKYs with or without treatment were isolated by ultracentrifugation and visualized by TEM after negative staining. The EVs isolated from four experimental groups were defined with different abbreviations (Fig. 3 A). Most of the SEVs exhibited intact diameters of <150 nm, consistent with a typical "cup-shaped" morphology for EVs (Fig. 3 A and B). The EV particles contained the established EV-associated protein markers, such as CD9, CD81, and Tsg101, but were negative for calnexin which is not expressed in EVs (Fig. 3 C) (Lyu et al., 2015). To verify the *in vivo* activity of serum EVs,

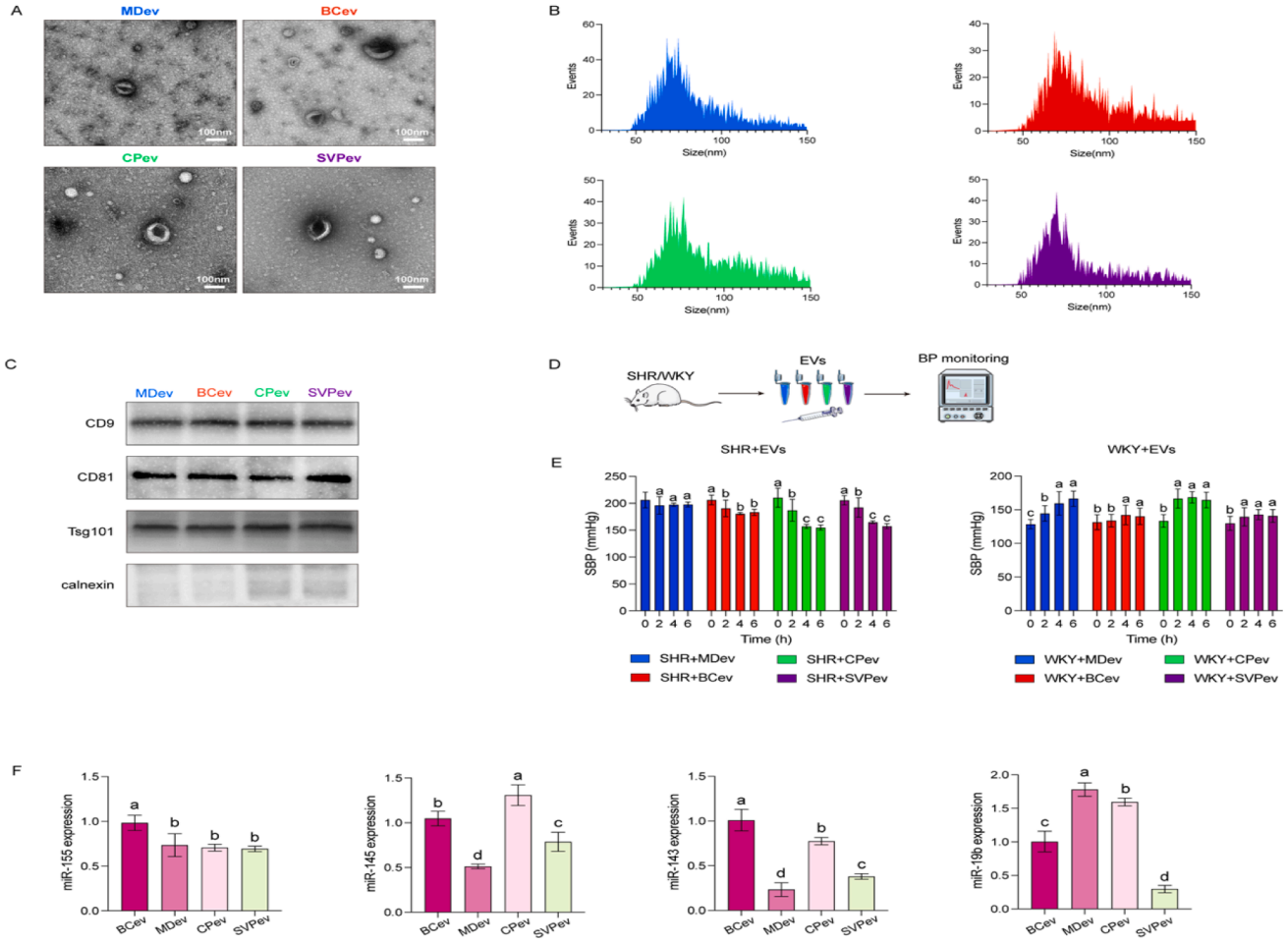


**Fig. 3. The characterization analysis and transplant of SHRs-derived serum extracellular vesicles.** (A) TEM analysis of EVs from four experimental group rats. Scale bar, 100 nm. (B) Particle sizes of four EVs samples were measured by an NTA analysis. (C) The expression of EV-specific markers CD9, CD81, and Tsg101 was measured with western blot analysis. (D) The schematic diagram of EVs-transplant. (E) The effects of four EVs samples on blood pressure of SHRs or WKYs within 6 h. (F) The expression of miRNA-155, miRNA-145, miRNA-143, and miRNA-19b in four serum EVs were tested by qRT-PCR. Values are expressed as mean ± SD (n = 6). Graph bars with different letters on top represent statistically significant results ($P < 0.05$) based on ANOVA analysis, whereas bars labeled with the same letter correspond to results that show no statistically significant differences.

some new rats which have not been treated with samples or drugs were regarded as recipients and were injected with four EVs samples. The BP was monitored for 6 h. Fig. 3 E showed that the BCev injection could slightly drop the SBP of SHRs within 6 h, while the CPev and SVPev also appeared a better hypotensive effect than that of BCev (decreased SBP to 157.42 ± 4.7 mmHg and 154.98 ± 4.8 mmHg, respectively). Intriguingly, the SBP of WKYs was increased through MDev, CPev, and SVPev treatment. The MDev enhanced SBP of WKYs from 128.66 ± 6.85 to 166.55 ± 11.43 mmHg, the CPev enhanced SBP from 133.45 ± 9.45 to 164.51 ± 11.51 mmHg, while the SVPev just increase SBP from 129.85 ± 7.51 to 140.87 ± 9.47 mmHg (Fig. 3 E). This result demonstrated that the serum EVs have *in vivo* physiological activity, and the SHRs-derived EVs could cause SBP to raise in WKYs, while the CPev and SVPev could decrease SBP of SHRs. It is a reasonable inference that a long-term CP or SVP intragastric administration could alter the bioactive macromolecules loaded in serum-EVs of SHRs. Hence, the miR-155, miR-145, miR-143, and miR-19b of different EVs samples were tested (Fig. 3 F). The CPev reversed the downregulation of miR-145 and miR-143 in the MDev, but the SVPev has a more significant improvement effect on the excessive upregulation of miR-19b. Associated with the results of the inflammatory cytokines in Fig. 2, we speculated that the response difference between SVP and CP to improving inflammation of the aorta should relate to miR-19b.

### 3.5. miR-19b regulate TRAF6 expression in the aorta via binding CYLD

To further reveal the molecular mechanism of miR-19b, the HUVECs were selected as a validator of vascular endothelial function. The CYLD, a deubiquitinating enzyme (DUBs), was predicted as a vital target of miR-19b according to the TargetScan database (https://www.targetscan.org/). The predicted location of the combination is in position 189–195 of CYLD 3'-UTR (Fig. 4 A). The mRNA and protein expression of CYLD in the aorta is detected to verify the negative regulatory relationship between miR-19b and CYLD. The results expressed that the CYLD mRNA in the aorta of the MD group was significantly lower than that in the BC group, and this phenomenon did not disappear after oral gastric captopril (Fig. 4 B). But the SVP significantly upregulated mRNA expression of CYLD in SHR, especially at a high concentration gavage. The western blot confirmed a similar perspective. The protein expression of CYLD in the MD group was significantly lower than that in the BC group, while the expression of CYLD in the SVP group was significantly upregulated (Fig. 4 C). The TRAF6A, a crucial target in the pro-inflammatory NF-κB signaling pathway, was simultaneously detected as a deubiquitinating substrate of CYLD (Trompouki et al., 2003). The results showed a negative mechanism between CYLD and TRAF6 in the aorta (Fig. 4 C). Subsequently, the dual-luciferase reporter assay was performed in the HUVECs with miR-19b mimic transfection. Firefly luciferase activity was significantly inhibited when transfected with

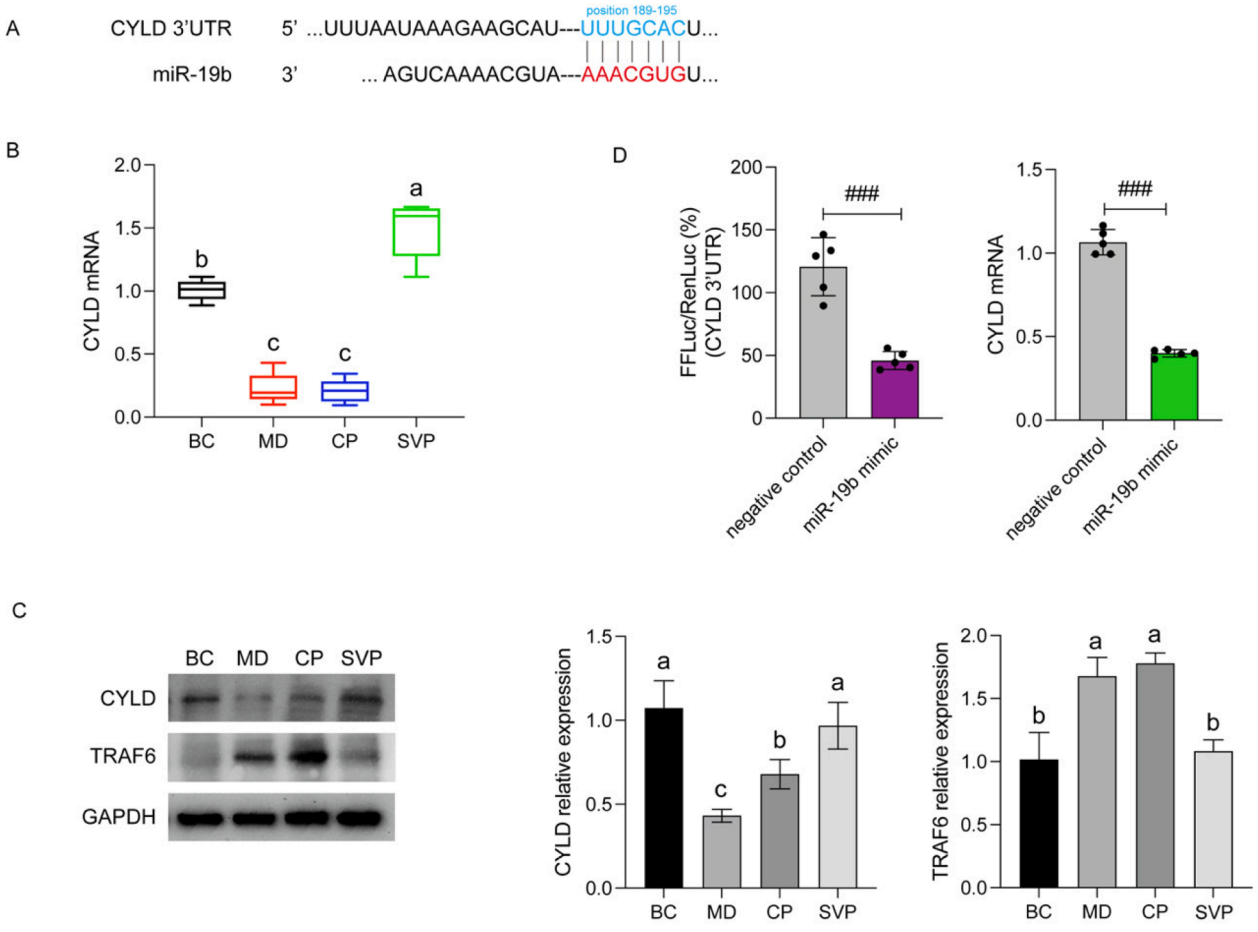


**Fig. 4. The SVP reduced TNF receptor-associated factor (TRAF) 6 expressions by regulating the serum EVs loading miRNA-19b targeting the CYLD expression in the aorta of SHRs.** (A) The binding position between miRNA-19b and CYLD was achieved from the TargetScan database. (B) The mRNA expression of CYLD in the aorta of rats was detected by qRT-PCR. (C) The SVP regulated the deubiquitination between CYLD and TRAF6 in the HUVECs. The protein expression was calculated by Image J software. (D) The targeted binding between miRNA-19b and CYLD was verified by a dual-luciferase reporter assay. The mRNA relative expression of CYLD in the HUVECs with miRNA-19b mimic or negative control miRNA incubation was quantitated (n = 5). Values are expressed as mean ± SD. ### represented $P < 0.05$; Graph bars with different letters on top represent statistically significant results ($P < 0.05$) based on ANOVA analysis, whereas bars labeled with the same letter correspond to results that show no statistically significant differences.

miR-19b mimic, indicating the CYLD is a target of miR-19b (Fig. 4 D). Similar binding mechanisms of miR-19b on CYLD were observed in previous studies (Nejad, Stunden, & Gantier, 2018; Ye et al., 2012). This result suggested that the SVP might improve inflammation of the aorta in SHRs by regulating the miR-19b-mediated deubiquitination of TRAF6.

### 3.6. EVs regulated inflammatory response of HUVECs

To confirm whether HUVECs uptake the EVs, four serum EV samples were labeled with a red fluorescent marker (PKH26) and incubated with HUVECs. After 12 h incubation, the cytoskeleton was stained with phalloidin (green) and the nucleus with DAPI (blue), and then analyzed by microscopy. The results showed the EVs samples could be internalized into HUVECs (Fig. 5 A). The ELISA assay suggested that the MDev significantly increased IL-6 and TNF- α of HUVECs to 743.71 ± 25.63 and 676.85 ± 18.63 pg/ml contrast with BCev (Fig. 5 B). Similar to the MDev, CPev also promoted the production of IL-6 and TNF- α in HUVECs (Fig. 5 B). The western blotting suggested that the expression CYLD in the HUVECs with MDev incubation is down-regulated, resulting in the cessation of ubiquitination degradation of TRAF6 (Fig. 5 C). The excessive accumulation of TRAF6 played a crucial role in mediating the inflammatory signaling pathway. MDev incubation significantly increased the phosphorylation of IκBα and induced the NF-κB signaling pathway activation (Fig. 5D). As shown in Fig. 5 D, the nuclear content of NF-κB p65 in HUVECs was increased by MDev incubation, while the cytoplasmic level of NF-κB was significantly decreased. This result further indicated that the MDev could significantly promote the nuclear translocation of NF-κB in endothelial cells (Fig. 5 D). The SVPev incubation could decrease the excessive accumulation of TRAF6 in the

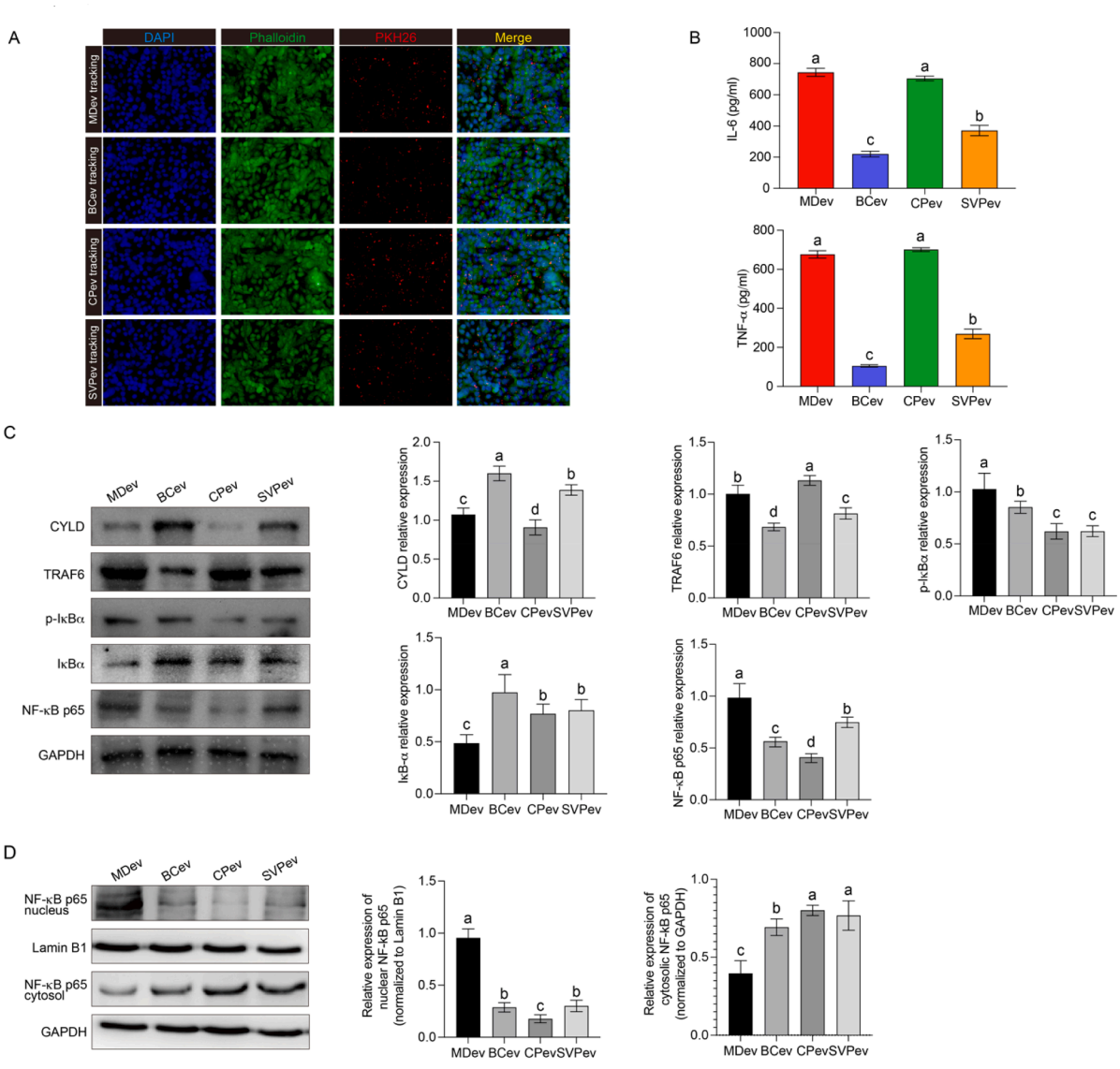


2

**Fig. 5. The serum EVs from rats with SVP gavage attenuated the endothelial inflammation by regulating the CYLD/TRAF6/NF-κB axis.** (A) The microscopic images showed uptake of the serum EVs from rats by the HUVECs. The cell nuclei were stained by DAPI in blue, the cytoskeleton was stained by phalloidin in green, and the EVs were stained by PKH26 in red. (B) The inflammatory cytokine IL-6 and TNF-α of HUVECs with different EVs incubation were tested by ELISA. (C) The protein expression of the CYLD/TRAF6/NF-κB axis in the HUVECs with EVs incubation was detected by western blot. (D) The protein expression of nuclear and cytosolic NF-κB p65 in the HUVECs EVs incubation was detected by western blot. Values are expressed as mean ± SD. Graph bars with different letters on top represent statistically significant results ($P < 0.05$) based on ANOVA analysis, whereas bars labeled with the same letter correspond to results that show no statistically significant differences. (For interpretation of the references to colour in this figure legend, the reader is referred to the web version of this article.)

HUVECs by reinstating the expression of CYLD, which is consistent with experimental results of inflammatory factors.

### 3.7. The effect of CYLD knockout on inflammation of HUVECs

To investigate the potential role of CYLD in endothelial inflammation, the CYLD siRNAs were used to knockdown the CYLD expression in the HUVECs. Two different siRNAs were performed to target the CYLD. Both of them were observed to knockout the CYLD effectively in the HUVECs (Fig. 6 A). Transfection of the endothelial cells with CYLD siRNAs significantly improved the TRAF6 expression contrast with the siControl group (Fig. 6 A). And not only that, but the HUVECs with siCYLD incubation also promoted the expression of p-IκBα and NF-κB p65. The siCYLD transfection could remarkably elevate the level of pro-inflammatory cytokine IL-6 and TNF-α in the HUVECs (Fig. 6 D). Hence, the results confirmed that the loss of CYLD could cause an increase in the inflammatory response of HUVECs.

## 4. Discussion

Cardiovascular disease (CVD) is considered a crucial health disorder as its prevalence in the world. Cardiovascular dysfunction has been found in a variety of pathological diseases including hypertension, hyperlipidemia, and diabetes (Wong, Tsai, Ip, & Irwin, 2018). Those pathological cases are confirmed to be important risk factors for inducing vascular function damage and inflammation, further promoting cardiovascular disease (Daiber & Chlopicki, 2020). Numerous vasoprotective therapies based on anti-inflammation and/or anti-oxidants have been confirmed to be prominent effective for improvement in CVD. The VECs and VSMCs are the most important components of the vascular wall. They are often regarded as regulators of the vascular microenvironment due to the loading of many receptor proteins and ion channels (Guo et al., 2018). The overactivated RAAS could induce abundant Ang II production, which promotes the phenotypic switch and metabolic alterations of VECs and VSMCs (Patel, Rauf, Khan, & Abu-Izneid, 2017). Previous studies in our lab suggested that the Ang II could modify the physiological state of vascular cells by altering the extracellular vesicles of VECs and VSMCs (Song, Lv, Zhang, et al., 2020; Song et al., 2021). The Ang II-induced VECs secreted a special EV packaging some special biomacromolecules such as miRNAs and proteins. Then the VECs-derived EVs were internalized into VSMCs and cased pathological response, and vice versa. However, the working mechanism of this process *in vivo* is still unclear. This study focused on vascular inflammation in SHRs and verified the presence of a potential EVs-mediated signaling pathway.

The hydrolysates derived from soybean protein have displayed a series of profitable activities, especially for CVD system (Guan, Diao, Jiang, Han, & Kong, 2018; H. Y. Yang, Yang, Chen, & Chen, 2008). With the continuous development of chromatography and mass spectrometry technology, more and more bioactive peptides are being identified from

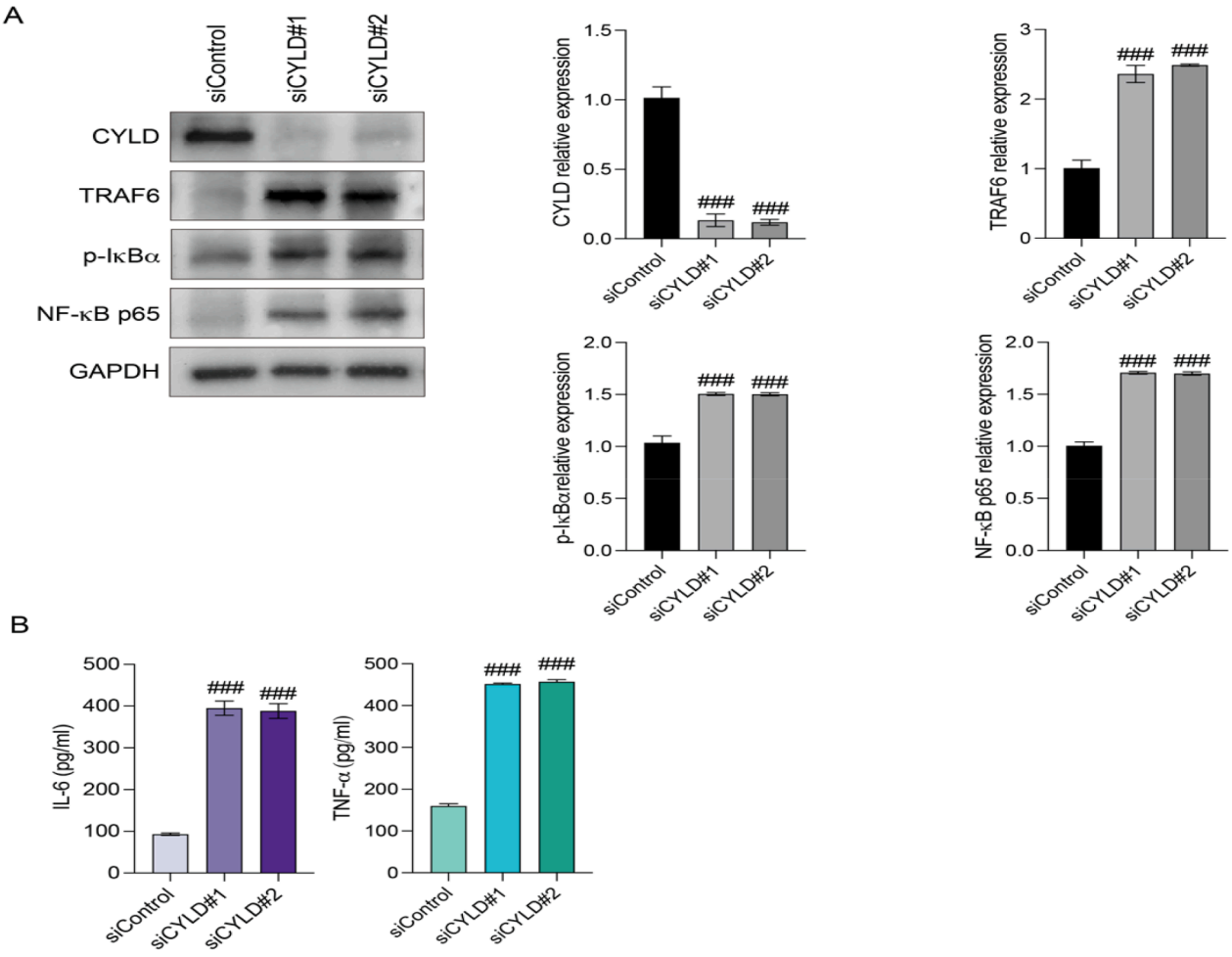


**Fig. 6. The effects of knockout treatment on the CYLD/TRAF6/NF-kB axis in the HUVECs.** (A) The protein expression of TRAF6, p-IκBα, and NF-κB p65 in the HUVECs with siRNA-CYLD (siCYLD) or siRNA-negative control (siControl) was detected. The immunoblotting images were represented as repetitive bands. (B) The inflammatory cytokine IL-6 and TNF-α of HUVECs with CYLD knockout treatment were tested by ELISA. Values are expressed as mean ± SD. ### represented $P < 0.05$.

soybean hydrolysate. However, the research on soybean protein-derived biopeptide in the *in vivo* anti-inflammatory activity is still in its infancy. Followed by our previous study, the soybean protein hydrolysate was prepared by alcalase, and various physicochemical operations including membrane separation, ethanol precipitation, and adsorption chromatography enrichment were used to purify the biopeptide (Xu et al., 2021). Results from this study further indicated that the soybean protein-derived vasoactive peptides (SVP) have an obvious effect on lowering blood pressure and improving the inflammation of the aorta in the SHRs. The captopril is a recognized medication used in the management of hypertension due to its ACE inhibition activity. The SHRs were orally administrated with captopril or SVP in current study. The dose of captopril was referred to be equivalent to 200 mg for human according to instruction. The hydrolysate was orally administrated to SHRs at dose of 100 and 500 mg/kg·BW referred to the human equivalent dose based on body surface. Compared with captopril, the SVP showed a more significant hypotensive effect at high concentration doses (500 mg/kg·BW) referred to as maximum protein intake (Wu, 2016), while there was no significant effect on blood pressure in the normotensive WKYs (Fig. 1). Interestingly, there was a slight increase in BP of WKY after long-term captopril (no significant difference in statistics) (Fig. 1 D and E). It has been demonstrated that a long-term administration with ACE inhibitors could elevate the plasmatic ACE concentration in rats, which might be an adaptive response to the inhibition of ACE activity in rats (Mas-Capdevila et al., 2019). It is worth noting that in the pre-protection experiment, the WKYs with SVP intragastric administration had a more gradual rise in BP after being injected with Ang II (Fig. 1 F), which might imply the SVP is a potential vascular protector.

A recent study indicated that the $H_2S$ arrested the development of hypertension by reducing vascular inflammation (Jin & DU, 2008). The development of vascular inflammation is usually accompanied by the production of vascular remodeling (Virdis et al., 2014). The SVP decreased the pro-inflammation cytokines IL-6 and TNF- α in serum and aorta of SHR (Fig. 1 G and Fig. 2 H). Consistent with this result, the histopathology also showed that SVP administration could attenuate the inflammatory cell infiltration and decrease the thickness of the vascular wall (Fig. 2 D). In a previous study, the Tongxinluo, a traditional Chinese medicine, was investigated to exert vasoprotective effects by blunting an Akt1-mediating feedback pathway between miR-155 and TNF-α (R. N. Zhang et al., 2014). Aspirin has been reported to prevent TNF-α-induced endothelial dysfunction by regulating the NF-κB-dependent miR-155/eNOS pathway (J. Kim et al., 2017). The miR-145 and miR-143 have been verified to regulate the phenotype switch of VSMCs (Chung et al., 2020; Rangrez, Massy, Meuth, & Metzinger, 2011). However, we noted that these miRNAs in the aortic of the SVP group had no excellent regulatory differences compared to the miR-19b (Fig. 3 F). Therefore, the miR-19b may be more closely related to the *in vivo* function of SVP.

The extracellular vesicles have increasingly been considered a vital carrier of miRNA molecules in the circulatory system. In the present study, the EVs were isolated from WKYs and SHRs and named as BCev, MDev, CPev, and SVPev according to the experimental group. The morphological characteristics, particle size, and the biomarker were identified by TEM, NTA, and western blot analysis (Fig. 3 A, B, and C). Subsequently, the EVs samples were transplanted into SHRs and WKYs, the BP was continuously monitored for 6 h. We found that the SHR-derived EVs were able to increase the SBP of WKYs, but the SVPev had the weakest blood pressure-raising effect (Fig. 3 E). Both CPev and SVPev reduced the SBP of SHRs within 6 h. Previous studies have reported that intravenous injection of SHR-derived EVs upgraded the BP and vascular ACE contents, and induced vascular remodeling, while WKY-EVs possessed a contrary effect on SHRs, and our conclusions are consistent with it (Ren et al., 2020). The miRNAs of EVs were quantified, and results exhibited that the miR-19b has the largest difference threshold in SVPev contrasted with other EVs. The packaging capacity of CPev for miR-145 and miR-143 was significantly stronger than that of SVPev. This conclusion indicated that captopril and SVP have different EVs-mediating mechanisms for vascular inflammation.

A clinical study showed that the miR-19b was related to myocardial fibrosis and regulated connective tissue growth factor protein and lysyl oxidase (LOX) protein, which suggested the serum miR-19b should be a biomarker of the myocardial collagen network (Beaumont et al., 2017). The VEC-derived microvesicles carrying miR-19b enrichment could inhibit VECs proliferation and migration by targeting Rho GTPase-activating protein 5 (ARHGAP5) and transforming growth factor β 2 (TGFβ2), which modulated the endothelial function (Shu, Tan, Miao, & Zhang, 2019). These studies release an obvious announcement that the miR-19b can be transmitted by extracellular vesicles and plays an important role in the circulatory system. In this study, the cylindromatosis (CYLD), an important target of miR-19b, was verified to be responsible for the regulation of the SVPev (Fig. 4). Gao et al. reported that the CYLD as a deubiquitinase controls the migration of the endothelial cells by activating Rac1 (Gao et al., 2010). Furthermore, the CYLD-TRAF6 interaction has been published to be a master modulation mechanism for multiple signaling pathways associated with vascular function (Mao et al., 2017; Trompouki et al., 2003). It is a consistent conclusion with those previous studies, that is the CYLD was significantly downregulated in the aorta of SHRs in contrast with WKY, but SVP not CP was profitable for this process (Fig. 4 B and C). The negative feedback relationship between CYLD and TRAF6 was proved to exist in the aorta of SHR (Fig. 4 C). Transfection by miR-19b mimic confirmed that HUVEC is a suitable model for studying the molecular function of CYLD, due to its presence in the regulatory network of miR-19b with CYLD (Fig. 4 D). Hence, the HUVECs were used to verify the physiological function of serum-derived EVs.

Internalization into cells is a necessary condition for exerting the regulation effects of EVs on the receptor. A series of staining labeling assays demonstrated the process by which EVs enter the HUVECs (Fig. 5 A). Although there was no obvious difference in the ability of the four EVs to enter HUVECs, the expression of inflammatory factors was significantly different. A previous study demonstrated that the VSMCs, in response to adverse stimuli such as oxLDL exposure, released some miR-155-rich EVs into the surrounding microenvironment, which internalized into VECs and triggered the endothelial dysfunction (Zheng et al., 2017). The SHR-derived EVs (MDev) were defined as miR-19b-enriched EVs that could inhibit the expression of CYLD via being captured with HUVECs. Inhibition of CYLD caused excessive accumulation of TRAF6 in endothelial cells, which in turn triggered endothelial IL-6 and TNF- α production (Fig. 5 B and C). In Fig. 5C, the MDev (serum EVs from SHRs) group showed p-IκBα up-regulation, the p-IκBα is then ubiquitinated by the ubiquitin ligase P-TrCP, which can be recognized and degraded by the 26S proteasome. Then NF-κB can be released from the cytoplasmic NF-κB/IκBα complex, and activate and expose the nuclear localization domain to form a dimer, which rapidly undergoes nuclear translocation. Hence, this phenomenon indicated that the NF-κB signaling was activated in MDev group. Importantly, the MDev could significantly promote the nuclear translocation of NF-κB in endothelial cells, this might be direct evidence that the MDev could active the NF-κB signaling pathway in endothelial cells. However, the EVs from SHR with SVP treatment did not exhibit excessive accumulation of miR-19b, so the SVPev was released in the vascular microenvironment and did not overact the inflammatory cytokine secretion. The CYLD plays a vital role in this process. Hence, the gene knockout experiment confirmed that the expression of TRAF6 was upregulated in the HUVECs with CYLD knockout (Fig. 6). Although the signaling mechanism of TRAF6 has been extensively studied in the TLR and IL-1R pathways, the way of TRAF6 mediated-downstream pathways is still unclear (Kanayama et al., 2004). The self-ubiquitinated TRAF6 was found to assemble a signaling complex that facilitates TAK1 and IKK activation by recruiting the downstream kinases TAK1 and IKK (Shi & Sun, 2018). Some studies reported that the TRAF6 autoubiquitination might be dispensable for activation of TAK1 and its downstream NF-κB and MAPK pathways, but the TRAF6-

mediated NEMO ubiquitination could promote the activation of IκB-α and NF-κB p65 (Ea, Deng, Xia, Pineda, & Chen, 2006). Although the TRAF6 ubiquitination degradation is generally believed to be essential for its signaling function, there are controversies. Some studies indicated that the expression of TRAF6 only partially inhibits its function in mediating activation of NF-κB and MAPK signaling stimulated by IL-1, TLRs, and RANKL. Hence, the manuscript would like to elaborate the SVP could intervene in the inflammatory level of the aorta in SHRs by regulating CYLD expression. (L. M. Zhang, Zhou, & Luo, 2018).

In conclusion, the present study demonstrated that the SVP and captopril treatment could lower blood pressure in SHR and improve vascular inflammation, but both mechanisms were significantly different. The SHR-derived miR-19b-rich EVs raised the SBP of WKY *in vivo* and increase the inflammatory response of HUVECs *in vitro*. However, the loading level of miR-19b in EVs derived from SVP-treated SHR returned to normal and did not exhibit pro-inflammatory activity in the HUVECs. The pro-inflammatory effect of miR-19b was verified to reduce the expression of CYLD in vascular endothelial cells, and the CYLD suppression further resulted in excessive accumulation of TRAF6 (a substrate of CYLD) in endothelial cells. A novel *in vivo* anti-inflammatory effect of SVP may be exerted by restoring the loading level of miR-19b in the EVs. Nevertheless, it should be noted that the SVP is a mixture containing abundant biopeptides, the identification of biopeptides should be worthy of attention.

## CRediT authorship contribution statement

**Tianyuan Song:** Conceptualization, Methodology, Writing – original draft, Writing – review & editing, Visualization. **Minzhi Zhou:** Conceptualization, Investigation. **Wen Li:** Investigation, Software. **Miao Lv:** Investigation, Validation. **Lin Zheng:** Conceptualization, Supervision, Writing – review & editing. **Mouming Zhao:** Conceptualization, Supervision, Writing – review & editing.

## Declaration of Competing Interest

The authors declare that they have no known competing financial interests or personal relationships that could have appeared to influence the work reported in this paper.

## Acknowledgement

This work was financially supported by the Key-Area Research and Development Program of Guangdong Province (2022B0202030001), the Key-Area Research and Development Program of Guangdong Province (2021B0707060001), Self-innovation Research Funding Project of Hanjiang Laboratory (HJL202101B001) and Shandong Provincial Key R&D Program (LJNY202018).

## References

Andaluz Aguilar, H., Iliuk, A. B., Chen, I. H., & Tao, W. A. (2019). Sequential phosphoproteomics and N-glycoproteomics of plasma-derived extracellular vesicles. *Nature Protocols*. https://doi.org/10.1038/s41596-019-0260-5

Barati, M., Javanmardi, F., Mousavi Jazayeri, S. M. H., Jabbari, M., Rahmani, J., Barati, F., … Mousavi Khaneghah, A. (2020). Techniques, perspectives, and challenges of bioactive peptide generation: A comprehensive systematic review. *Comprehensive Reviews in Food Science and Food Safety, 19*(4), 1488–1520. https://doi.org/10.1111/1541-4337.12578

Beaumont, J., López, B., Ravassa, S., Hermida, N., José, G. S., Gallego, I., … González, A. (2017). MicroRNA-19b is a potential biomarker of increased myocardial collagen cross-linking in patients with aortic stenosis and heart failure. *Scientific Reports*, *7* (December 2016), 1–10. https://doi.org/10.1038/srep40696.

Bodega, G., Alique, M., Puebla, L., Carracedo, J., & Ramírez, R. M. (2019). Microvesicles: ROS scavengers and ROS producers. *Journal of Extracellular Vesicles, 8*(1), 1626654. https://doi.org/10.1080/20013078.2019.1626654

Chatterjee, C., Gleddie, S., & Xiao, C. W. (2018). Soybean bioactive peptides and their functional properties. *Nutrients*. https://doi.org/10.3390/nu10091211

Chung, D. J., Wu, Y. L., Yang, M. Y., Chan, K. C., Lee, H. J., & Wang, C. J. (2020). Nelumbo nucifera leaf polyphenol extract and gallic acid inhibit TNF-α-induced vascular smooth muscle cell proliferation and migration involving the regulation of miR-21, miR-143 and miR-145. *Food and Function (Vol. 11)*. https://doi.org/10.1039/d0fo02135k.

Daiber, A., & Chlopicki, S. (2020). Revisiting pharmacology of oxidative stress and endothelial dysfunction in cardiovascular disease: Evidence for redox-based therapies. *Free Radical Biology and Medicine, 157*(February), 15–37. https://doi.org/10.1016/j.freeradbiomed.2020.02.026

Ea, C.-K., Deng, L., Xia, Z.-P., Pineda, G., & Chen, Z. J. (2006). Activation of IKK by TNFα requires site-specific ubiquitination of RIP1 and polyubiquitin binding by NEMO. *Molecular Cell, 22*(2), 245–257.

Fang, T., Lv, H., Lv, G., Li, T., Wang, C., Han, Q., … Wang, H. (2018). Tumor-derived exosomal miR-1247-3p induces cancer-associated fibroblast activation to foster lung metastasis of liver cancer. *Nature Communications, 9*(1), 1–13. https://doi.org/10.1038/s41467-017-02583-0

Gao, J., Sun, L., Huo, L., Liu, M., Li, D., & Zhou, J. (2010). CYLD regulates angiogenesis by mediating vascular endothelial cell migration. *Blood, 115*(20), 4130–4137. https://doi.org/10.1182/blood-2009-10-248526

García-Tejedor, A., Manzanares, P., Castelló-Ruiz, M., Moscardó, A., Marcos, J. F., & Salom, J. B. (2017). Vasoactive properties of antihypertensive lactoferrin-derived peptides in resistance vessels: Effects in small mesenteric arteries from SHR rats. *Life Sciences, 186*(August), 118–124. https://doi.org/10.1016/j.lfs.2017.07.036

Gu, Y., & Wu, J. (2013). LC-MS/MS coupled with QSAR modeling in characterising of angiotensin I-converting enzyme inhibitory peptides from soybean proteins. *Food Chemistry, 141*(3), 2682–2690. https://doi.org/10.1016/j.foodchem.2013.04.064

Guan, H., Diao, X., Jiang, F., Han, J., & Kong, B. (2018). The enzymatic hydrolysis of soy protein isolate by Corolase PP under high hydrostatic pressure and its effect on bioactivity and characteristics of hydrolysates. *Food Chemistry, 245*, 89–96. https://doi.org/10.1016/j.foodchem.2017.08.081

Guo, Y., Yang, X., He, J., Liu, J., Yang, S., & Dong, H. (2018). Important roles of the Ca2+-sensing receptor in vascular health and disease. *Life Sciences, 209*(April), 217–227. https://doi.org/10.1016/j.lfs.2018.08.016

Han, Y., Zhang, J., Huang, S., Cheng, N., Zhang, C., Li, Y., … Du, J. (2021). MicroRNA-223-3p inhibits vascular calcification and the osteogenic switch of vascular smooth muscle cells. *Journal of Biological Chemistry, 296*, Article 100483. https://doi.org/10.1016/j.jbc.2021.100483

Hergenreider, E., Heydt, S., Tréguer, K., Boettger, T., Horrevoets, A. J. G., Zeiher, A. M., … Dimmeler, S. (2012). Atheroprotective communication between endothelial cells and smooth muscle cells through miRNAs. *Nature Cell Biology, 14*(3), 249–256. https://doi.org/10.1038/ncb2441

Hu, M., Jia, F., Huang, W. P., Li, X., Hu, D. F., Wang, J., … Ji, J. (2021). Substrate stiffness differentially impacts autophagy of endothelial cells and smooth muscle cells. *Bioactive Materials, 6*(5), 1413–1422. https://doi.org/10.1016/j.bioactmat.2020.10.013

Jin, H., Sun, Y., Liang, J., Tang, C., & DU, J. (2008). Hypotensive effects of hydrogen sulfide via attenuating vascular inflammation in spontaneously hypertensive rats. *Zhonghua xin xue guan bing za zhi*, *36*(6), 541–545. Retrieved from http://europepmc.org/abstract/MED/19100070.

Kanayama, A., Seth, R. B., Sun, L., Ea, C.-K., Hong, M., Shaito, A., … Chen, Z. J. (2004). TAB2 and TAB3 activate the NF-κB pathway through binding to polyubiquitin chains. *Molecular Cell, 15*(4), 535–548.

Kim, I. S., Yang, W. S., & Kim, C. H. (2021). Beneficial effects of soybean-derived bioactive peptides. *International Journal of Molecular Sciences, 22*(16), 1–23. https://doi.org/10.3390/ijms22168570

Kim, J., Lee, K. S., Kim, J. H., Lee, D. K., Park, M., Choi, S., … Kim, Y. M. (2017). Aspirin prevents TNF-α-induced endothelial cell dysfunction by regulating the NF-κB-dependent miR-155/eNOS pathway: Role of a miR-155/eNOS axis in preeclampsia. *Free Radical Biology and Medicine*, *104*(December 2016), 185–198. https://doi.org/10.1016/j.freeradbiomed.2017.01.010.

La Salvia, S., Gunasekaran, P. M., Byrd, J. B., & Erdbrügger, U. (2020). Extracellular vesicles in essential hypertension: Hidden messengers. *Current Hypertension Reports, 22*(10). https://doi.org/10.1007/s11906-020-01084-8

Lin, Q., Liao, W., Bai, J., Wu, W., & Wu, J. (2017). Soy protein-derived ACE-inhibitory peptide LSW (Leu-Ser-Trp) shows anti-inflammatory activity on vascular smooth muscle cells. *Journal of Functional Foods, 34*, 248–253. https://doi.org/10.1016/j.jff.2017.04.029

Liu, H., Liang, J., Zhong, Y., Xiao, G., Efferth, T., Georgiev, M. I., … Wang, Q. (2021). Dendrobium officinale Polysaccharide Alleviates Intestinal Inflammation by Promoting Small Extracellular Vesicle Packaging of miR-433-3p. *Journal of Agricultural and Food Chemistry, 69*(45), 13510–13523. https://doi.org/10.1021/acs.jafc.1c05134

Liu, Y., Li, C., Wu, H., Xie, X., Sun, Y., & Dai, M. (2018). Paeonol attenuated inflammatory response of endothelial cells via stimulating monocytes-derived exosomal microRNA-223. *Frontiers in Pharmacology, 9*(NOV), 1–12. https://doi.org/10.3389/fphar.2018.01105

Lyu, L., Wang, H., Li, B., Qin, Q., Qi, L., Nagarkatti, M., … Cui, T. (2015). A critical role of cardiac fibroblast-derived exosomes in activating renin angiotensin system in cardiomyocytes. *Journal of Molecular and Cellular Cardiology, 89*, 268–279. https://doi.org/10.1016/j.yjmcc.2015.10.022

Mao, K., Shu, W., Liu, L., Gu, Q., Qiu, Q., & Wu, X. W. (2017). Salvianolic Acid A Inhibits OX-LDL Effects on Exacerbating Choroidal Neovascularization via Downregulating CYLD. *Oxidative Medicine and Cellular Longevity, 2017*. https://doi.org/10.1155/2017/6210694

Mas-Capdevila, A., Iglesias-Carres, L., Arola-Arnal, A., Suarez, M., Muguerza, B., & Bravo, F. I. (2019). Long-term administration of protein hydrolysate from chicken feet induces antihypertensive effect and confers vasoprotective pattern in diet-

induced hypertensive rats. *Journal of Functional Foods*, *55*(September 2018), 28–35. https://doi.org/10.1016/j.jff.2019.02.006.
Nair, A., & Jacob, S. (2016). A simple practice guide for dose conversion between animals and human. *Journal of Basic and Clinical Pharmacy, 7*(2), 27. https://doi.org/10.4103/0976-0105.177703
Nejad, C., Stunden, H. J., & Gantier, M. P. (2018). A guide to miRNAs in inflammation and innate immune responses. *FEBS Journal, 285*(20), 3695–3716. https://doi.org/10.1111/febs.14482
Osada-Oka, M., Shiota, M., Izumi, Y., Nishiyama, M., Tanaka, M., Yamaguchi, T., … Iwao, H. (2017). Macrophage-derived exosomes induce inflammatory factors in endothelial cells under hypertensive conditions. *Hypertension Research, 40*(4), 353–360. https://doi.org/10.1038/hr.2016.163
Pan, X., Shao, Y., Wu, F., Wang, Y., Xiong, R., Zheng, J., … Lin, Z. (2018). FGF21 Prevents Angiotensin II-Induced Hypertension and Vascular Dysfunction by Activation of ACE2/Angiotensin-(1–7) Axis in Mice. *Cell Metabolism, 27*(6), 1323–1337.e5. https://doi.org/10.1016/j.cmet.2018.04.002
Paolicelli, R. C., Bergamini, G., & Rajendran, L. (2019). Cell-to-cell Communication by Extracellular Vesicles: Focus on Microglia. *Neuroscience, 405*(April), 148–157. https://doi.org/10.1016/j.neuroscience.2018.04.003
Patel, S., Rauf, A., Khan, H., & Abu-Izneid, T. (2017). Renin-angiotensin-aldosterone (RAAS): The ubiquitous system for homeostasis and pathologies. *Biomedicine and Pharmacotherapy, 94*, 317–325. https://doi.org/10.1016/j.biopha.2017.07.091
Rangrez, A. Y., Massy, Z. A., Le Meuth, V. M., & Metzinger, L. (2011). MiR-143 and miR-145 molecular keys to switch the phenotype of vascular smooth muscle cells. *Circulation: Cardiovascular Genetics, 4*(2), 197–205. https://doi.org/10.1161/CIRCGENETICS.110.958702
Reiner, A. T., & Somoza, V. (2019). Extracellular vesicles as vehicles for the delivery of food bioactives. *Journal of Agricultural and Food Chemistry, 67*(8), 2113–2119. https://doi.org/10.1021/acs.jafc.8b06369
Ren, X. S., Tong, Y., Qiu, Y., Ye, C., Wu, N., Xiong, X. Q., … Zhu, G. Q. (2020). MiR155-5p in adventitial fibroblasts-derived extracellular vesicles inhibits vascular smooth muscle cell proliferation via suppressing angiotensin-converting enzyme expression. *Journal of Extracellular Vesicles, 9*(1). https://doi.org/10.1080/20013078.2019.1698795
Shi, J. H., & Sun, S. C. (2018). Tumor necrosis factor receptor-associated factor regulation of nuclear factor κB and mitogen-activated protein kinase pathways. *Frontiers in Immunology*. https://doi.org/10.3389/fimmu.2018.01849
Shu, Z., Tan, J., Miao, Y., & Zhang, Q. (2019). The role of microvesicles containing microRNAs in vascular endothelial dysfunction. *Journal of Cellular and Molecular Medicine*. https://doi.org/10.1111/jcmm.14716
Song, T., Lv, M., Sun, B., Zheng, L., & Zhao, M. (2020). Tripeptides Val-Pro-Pro (VPP) and Ile-Pro-Pro (IPP) regulate the proliferation and migration of vascular smooth muscle cells by interfering Ang II-induced human umbilical vein endothelial cells-derived EVs delivering RNAs to VSMCs in the co-culture model. *Journal of Agricultural and Food Chemistry*. https://doi.org/10.1021/acs.jafc.0c02060
Song, T., Lv, M., Zhou, M., Huang, M., Zheng, L., & Zhao, M. (2021). Soybean-Derived Antihypertensive Peptide LSW (Leu-Ser-Trp) Antagonizes the Damage of Angiotensin II to Vascular Endothelial Cells through the Trans-vesicular Pathway. *Journal of Agricultural and Food Chemistry, 69*(36), 10536–10549. https://doi.org/10.1021/acs.jafc.1c02733
Sun, X., Belkin, N., & Feinberg, M. W. (2013). Endothelial MicroRNAs and atherosclerosis. *Current Atherosclerosis Reports, 15*(12). https://doi.org/10.1007/s11883-013-0372-2
Taganov, K. D., Boldin, M. P., Chang, K. J., & Baltimore, D. (2006). NF-κB-dependent induction of microRNA miR-146, an inhibitor targeted to signaling proteins of innate immune responses. *Proceedings of the National Academy of Sciences of the United States of America, 103*(33), 12481–12486. https://doi.org/10.1073/pnas.0605298103
Trompouki, E., Hatzivassillou, E., Tsichritzis, T., Farmer, H., Ashworth, A., & Mosialos, G. (2003). CYLD is a deubiquitinating enzyme that negatively regulates NF-κB activation by TNFR family members. *Nature, 424*(6950), 793–796. https://doi.org/10.1038/nature01803
Tu, Z., Chen, L., Wang, H., Ruan, C., Zhang, L., & Kou, Y. (2014). Effect of fermentation and dynamic high pressure microfluidization on dietary fibre of soybean residue. *Journal of Food Science and Technology, 51*(11), 3285–3292. https://doi.org/10.1007/s13197-012-0838-1
Utsunomiya, H., Takaguri, A., Bourne, A. M., Elliott, K. J., Akazawa, S. I., Okuno, Y., … Eguchi, S. (2011). An extract from brown rice inhibits signal transduction of angiotensin II in vascular smooth muscle cells. *American Journal of Hypertension, 24*(5), 530–533. https://doi.org/10.1038/ajh.2011.10
Virdis, A., Dell'Agnello, U., & Taddei, S. (2014). Impact of inflammation on vascular disease in hypertension. *Maturitas, 78*(3), 179–183. https://doi.org/10.1016/j.maturitas.2014.04.012
Virdis, A., & Schiffrin, E. L. (2003). Vascular inflammation: a role in vascular disease in hypertension? *Current Opinion in Nephrology and Hypertension*, *12*(2). Retrieved from https://journals.lww.com/co-nephrolhypertens/Fulltext/2003/03000/Vascular_inflammation_a_role_in_vascular_disease.9.aspx.
Wong, D., Tsai, P. N. W., Ip, K. Y., & Irwin, M. G. (2018). New antihypertensive medications and clinical implications. *Best Practice and Research: Clinical Anaesthesiology, 32*(2), 223–235. https://doi.org/10.1016/j.bpa.2018.06.013
Wu, G. (2016). Dietary protein intake and human health. *Food and Function, 7*(3), 1251–1265. https://doi.org/10.1039/c5fo01530h
Xu, Z., Wu, C., Sun-Waterhouse, D., Zhao, T., Waterhouse, G. I. N., Zhao, M., & Su, G. (2021). Identification of post-digestion angiotensin-I converting enzyme (ACE) inhibitory peptides from soybean protein Isolate: Their production conditions and in silico molecular docking with ACE. *Food Chemistry*, *345*(October 2020), 128855. https://doi.org/10.1016/j.foodchem.2020.128855.
Yang, C., Wu, X., Shen, Y., Liu, C., Li, P., & Kong, X. (2020). Alamandine attenuates angiotensin II-induced vascular fibrosis via inhibiting p38 MAPK pathway. *European Journal of Pharmacology, 883*(June), Article 173384. https://doi.org/10.1016/j.ejphar.2020.173384
Yang, H. Y., Yang, S. C., Chen, S. T., & Chen, J. R. (2008). Soy protein hydrolysate ameliorates cardiovascular remodeling in rats with l-NAME-induced hypertension. *Journal of Nutritional Biochemistry, 19*(12), 833–839. https://doi.org/10.1016/j.jnutbio.2007.11.004
Ye, H., Liu, X., Lv, M., Wu, Y., Kuang, S., Gong, J., … Guo, A. Y. (2012). MicroRNA and transcription factor co-regulatory network analysis reveals miR-19 inhibits CYLD in T-cell acute lymphoblastic leukemia. *Nucleic Acids Research, 40*(12), 5201–5214. https://doi.org/10.1093/nar/gks175
Zhang, L. M., Zhou, J. J., & Luo, C. L. (2018). CYLD suppression enhances the pro-inflammatory effects and hyperproliferation of rheumatoid arthritis fibroblast-like synoviocytes by enhancing NF-κB activation. *Arthritis Research and Therapy, 20*(1), 1–13. https://doi.org/10.1186/s13075-018-1722-9
Zhang, R. N., Zheng, B., Li, L. M., Zhang, J., Zhang, X. H., & Wen, J. K. (2014). Tongxinluo inhibits vascular inflammation and neointimal hyperplasia through blockade of the positive feedback loop between miR-155 and TNF-α. *American Journal of Physiology - Heart and Circulatory Physiology, 307*(4), 552–562. https://doi.org/10.1152/ajpheart.00936.2013
Zheng, B., Yin, W. na, Suzuki, T., Zhang, X. hua, Zhang, Y., Song, L. li, … Wen, J. kun. (2017). Exosome-Mediated miR-155 Transfer from Smooth Muscle Cells to Endothelial Cells Induces Endothelial Injury and Promotes Atherosclerosis. *Molecular Therapy*, *25*(6), 1279–1294. https://doi.org/10.1016/j.ymthe.2017.03.031.
Zhu, L. L., Huang, X., Yu, W., Chen, H., Chen, Y., & Dai, Y. T. (2018). Transplantation of adipose tissue-derived stem cell-derived exosomes ameliorates erectile function in diabetic rats. *Andrologia, 50*(2), 1–9. https://doi.org/10.1111/and.12871